INORGANIC CHEMISTRY FRONTIERS

RESEARCH ARTICLE

View Article Online
View Journal | View Issue

Check for updates

Cite this: *Inorg. Chem. Front.*, 2025, **12**, 253

Magneto-optical response and luminescence properties of lanthanide–titanium–oxo clusters Eu_2Ti_7 and Sm_2Ti_7†

Wei-Dong Liu, Han Xu, Chong-Yang Li, La-Sheng Long, Lan-Sun Zheng and Xiang-Jian Kong *

The study of magneto-optical effects based on the f–f emission and absorption of lanthanide ions has attracted considerable interest. In this work, we present a series of isostructural lanthanide–titanium–oxo clusters (LTOCs) **Ln_2Ti_7** (Ln = La, Sm, Eu) using 3,5-di-*tert*-butylbenzoic acid as the ligand. A detailed comparison of the luminescence properties of **Sm_2Ti_7** and **Eu_2Ti_7** shows that **Eu_2Ti_7** displays superior luminescence intensity, higher color purity red light, longer lifetime, and significantly higher quantum yield. These properties, along with its high stability in solution, make **Eu_2Ti_7** an excellent candidate for magnetic circularly polarized luminescence (MCPL) studies. Under an external magnetic field, **Eu_2Ti_7** exhibited strong MCPL signals, with the maximum $|g_{MCPL}|$ value being 0.04 T^{-1} from the $^5D_0 \rightarrow {}^7F_4$ transition. In contrast, the weaker luminescence of **Sm_2Ti_7** rendered MCPL analysis ineffective; however, its strong near-infrared absorption allowed for magnetic circular dichroism (MCD) studies. The MCD spectra of Sm_2Ti_7 revealed significant signals corresponding to f–f transitions in the 900–1600 nm range, with the maximum $|g_{MCD}|$ value observed at 1102 nm. This work provides valuable insights into the magneto-optical properties of Ln-based clusters, emphasizing the role of energy-level analysis for further research into their potential applications in magneto-optical devices.

Received 20th October 2024,
Accepted 14th November 2024

DOI: 10.1039/d4qi02645d

rsc.li/frontiers-inorganic

Published on 21 November 2024. Downloaded on 5/17/2026 11:32:44 AM.

10th anniversary statement

It is a great honor to contribute to the 10th anniversary collection of this esteemed journal. I had the privilege of publishing a paper on lanthanide-oxo clusters in the *Emerging Investigator* themed collection of *Inorganic Chemistry Frontiers* in 2016 (*Inorg. Chem. Front.*, 2016, **3**, 320–325). Over the years, this journal has provided an invaluable platform for reporting groundbreaking research and encouraging collaborations within China, across Asia, and internationally. *Inorganic Chemistry Frontiers* has played a vital role in advancing the field of inorganic chemistry. I look forward to the journal's continued growth and influence.

Introduction

Most trivalent lanthanide ions possess a rich array of uniquely arranged electron energy levels, which result in characteristic f–f absorption and emission transitions.[1] These features make Ln(III) highly valuable in spectroscopy, particularly in the unique magneto-optical properties.[2] An external magnetic field can induce optical activity and magneto-optical effects in both achiral and optically inactive substances, such as the Faraday effect, Zeeman effect, and polar Kerr effect.[3] The interaction of light with matter in an external magnetic field is particularly noteworthy because it can lead to magnetic circular dichroism (MCD) in the ground state and magnetic circularly polarized luminescence (MCPL) in the excited state. This phenomenon arises from the Zeeman splitting in their degenerate ground and excited states of achiral and optically inactive substances.[4]

The design and synthesis of molecules containing Ln(III) with well-defined structure are essential for studying the magneto-optical effect of these ions.[5] In the selected molecular model for investigating the magneto-optical behavior of Ln(III), the MCPL and MCD signals of Ln(III) can be obtained by choosing suitable ligands, regulating the coordination environ-

State Key Laboratory of Physical Chemistry of Solid Surfaces, and Department of Chemistry, College of Chemistry and Chemical Engineering, Xiamen University, Xiamen 361005, China. E-mail: xjkong@xmu.edu.cn

†Electronic supplementary information (ESI) available. CCDC 2392362–2392364 and 2392375. For ESI and crystallographic data in CIF or other electronic format see DOI: https://doi.org/10.1039/d4qi02645d

Published on 21 November 2024. Downloaded on 5/17/2026 11:32:44 AM.

ment of Ln(III), and minimizing interference with f–f transitions.[6] The 3d–4f clusters have the characteristics of multiple metal centers, allowing for synergistic interactions between different metal ions.[7] However, 3d–4f clusters with both absorption and emission magneto-optical effects are extremely rare. Current studies of MCPL in lanthanide systems have mostly focused on mononuclear complexes,[8] with the exception of the Ln_{20} cluster,[9] and investigations into MCD in the near-infrared range remain limited.[10]

Lanthanide–titanium–oxo clusters (LTOCs) represent a distinct class of 3d–4f clusters. Their core structures, due to the presence of Ti(IV) with strong Lewis acidity, allow the metal ions to be commonly interconnected *via* O^{2-} bridges, which helps mitigate the negative impact of O–H stretching vibrations on Ln(III) luminescence.[11] By selecting efficient photosensitive ligands, LTOCs with excellent luminescence properties can be achieved.[12] These clusters have recently emerged as promising candidates for Ln(III)-based luminescent materials. Furthermore, since Ti(IV) lacks d-electrons, there are no d–d transitions in the absorption spectra, ensuring no interference with the f–f transitions of the lanthanide ions.[13] LTOCs provide new alternatives for the study of MCPL and MCD.

Herein, based on bis-*tert*-butyl modified carboxylic acid ligands, we report a series of lanthanide–titanium–oxo clusters, formulated as $Ln_2Ti_7(\mu_3\text{-}O)_6(L)_{14}(EtO)_8$ (**Ln_2Ti_7**, Ln = La, Sm, Eu; HL = 3,5-di-*tert*-butylbenzoic acid). The introduction of *tert*-butyl groups enhances the ligand sensitization effect and improves the solubility of the cluster. Luminescence studies reveal that **Eu_2Ti_7** exhibits superior luminescence properties compared to **Sm_2Ti_7**, with a longer lifetime and higher quantum yield. The excellent solubility and stability of the cluster in dichloromethane make it suitable for further MCPL study of **Eu_2Ti_7** and near-infrared MCD study of **Sm_2Ti_7**. Notably, achiral **Eu_2Ti_7** displays distinct and well-defined CPL signals in the external magnetic field. The energy level analysis prompted the study of the MCD of **Sm_2Ti_7** in the near-infrared region, which also yielded a signal with a near-ideal peak shape. This work marks the first investigation of both emission and absorption magneto-optical effects within the same 3d–4f cluster system.

Experimental section

Materials and physical measurements

All reagents were of analytical grade, commercially sourced, and were used without further purification. The crystallographic data were collected on a Rigaku Oxford diffraction XtaLAB synergy diffractometer with micro-focus sealed X-ray Cu Kα radiation (λ = 1.54184 Å) at 100 K. The excitation and emission spectra of the room-temperature luminescence, the time-resolved PL decay curves and the absolute quantum yields were measured on the steady-state and transient fluorescence spectrometer (FLS-1000, Edinburgh). Dynamic light scattering analysis was conducted using the laser particle size analyzer (Malvern, ZSU3100). The MCPL and MCD spectra were measured on the JASCO CPL-300 and JASCO J-1700 equipped with a JASCO PM-491 compact permanent magnet (1.6 T).

Synthesis of Ln_2Ti_7

Clusters **Ln_2Ti_7** (Ln = La, Sm, Eu) were synthesized through solvothermal crystallization by reacting $Ln(OAc)_3{\cdot}xH_2O$, Ti(O^iPr)$_4$, and 3,5-di-*tert*-butylbenzoic acid in ethanol. The solid reactants were fully dissolved by sonication in the sealed vials, followed by solvothermal reactions at 80 °C for 24–48 h. The colorless block crystals were obtained without cooling to room temperature, with yields exceeding 40% (calculated based on $Ln(OAc)_3{\cdot}xH_2O$).

Results and discussion

Single crystal structures

Single-crystal X-ray diffraction (SCXRD) analysis revealed that the three obtained clusters, $Ln_2Ti_7(\mu_3\text{-}O)_6(EtO)_8(L)_{14}$ (**Ln_2Ti_7**, Ln = La, Sm, Eu; HL = 3,5-di-*tert*-butylbenzoic acid), are electrically neutral and isostructural clusters, though their cell parameters differ. **La_2Ti_7** and **Sm_2Ti_7** crystallize in the triclinic crystal system with the space group $P\bar{1}$, while **Eu_2Ti_7** crystallizes in the monoclinic crystal system with the space group $C2/c$. To illustrate their structural features, we discuss in detail only the molecular structure of **La_2Ti_7**. As shown in Fig. 1a, the metal-oxo core $[La_2Ti_7(\mu_3\text{-}O)_6]^{22+}$ is stabilized by 14 L^- anions and 8 EtO^- anions. The metal-oxo core consists of two eight-

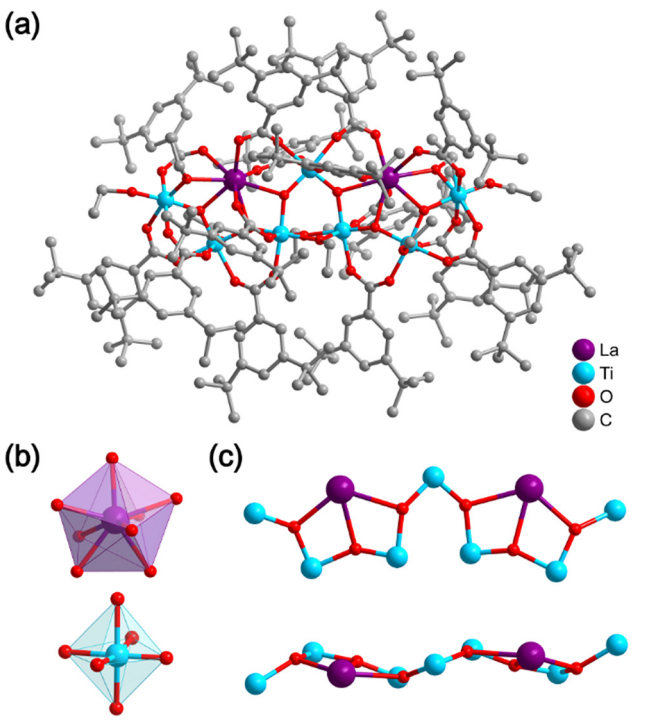

Fig. 1 (a) Crystal structure of **La_2Ti_7**. (b) Coordination configurations of La^{3+} ion and Ti^{4+} ion. (c) Ball-and-stick depiction of metal-oxo core $[La_2Ti_7(\mu_3\text{-}O)_6]^{22+}$.

This journal is © the Partner Organisations 2025

Published on 21 November 2024. Downloaded on 5/17/2026 11:32:44 AM.

coordinated La^{3+} ions and seven six-coordinated Ti^{4+} ions, connected by 6 μ_3-O^{2-} bridges (Fig. 1b and c). Interestingly, the previously reported cluster **LaTi$_4$**, obtained using benzoic acid ligands, features a $[LaTi_4(\mu_3\text{-}O)_3]^{13+}$ metal-oxo core (Fig. S2†).[14] The **La$_2$Ti$_7$** can be envisioned as two $[LaTi_4(\mu_3\text{-}O)_3]$ units sharing a Ti^{4+} ion in a "hand in hand" arrangement. In each $[LaTi_4(\mu_3\text{-}O)_3]$ unit, the four Ti^{4+} ions form a non-linear circular arc, with the La^{3+} surrounded by Ti^{4+} bridged through O^{2-} bridges. The bond distances and angles (Tables S5–S12†) are consistent with literature values. Notably, the molecular model of **Ln$_2$Ti$_7$** lacks OH^- bridges and features fourteen photosensitive ligands, making it suitable for luminescence studies.

Luminescence properties

Sm$_2$Ti$_7$ and **Eu$_2$Ti$_7$** were selected for luminescence studies due to energy levels of Sm(III) and Eu(III) favorable match with the chosen photosensitive ligands. Room-temperature luminescence measurements of **Sm$_2$Ti$_7$** and **Eu$_2$Ti$_7$** at room temperature were performed, with the results presented in Fig. 2. Fig. 2a displays the excitation and emission spectra of **Sm$_2$Ti$_7$**, which exhibits Sm(III) characteristic emission peaks at 562 nm ($^4G_{5/2} \rightarrow {}^6H_{5/2}$), 597 nm ($^4G_{5/2} \rightarrow {}^6H_{7/2}$), 644 nm ($^4G_{5/2} \rightarrow {}^6H_{9/2}$), and 706 nm ($^4G_{5/2} \rightarrow {}^6H_{11/2}$) upon irradiation at 339 nm or 405 nm ($^6H_{5/2} \rightarrow {}^6P_{3/2}$).[15] Fig. 2b presents the excitation and emission spectra of **Eu$_2$Ti$_7$**, where irradiation at 339 nm or 395 nm ($^7F_0 \rightarrow {}^5L_6$) leads to characteristic Eu(III) emissions at 580 nm ($^5D_0 \rightarrow {}^7F_0$), 593 nm ($^5D_0 \rightarrow {}^7F_1$), 618 nm ($^5D_0 \rightarrow {}^7F_2$), 650 nm ($^5D_0 \rightarrow {}^7F_3$) and 701 nm ($^5D_0 \rightarrow {}^7F_4$).[16] In Fig. 2c, the relative emission intensities of **Sm$_2$Ti$_7$** and **Eu$_2$Ti$_7$** are compared, along with a reference for emission peak widths. The luminescence of **Sm$_2$Ti$_7$** is primarily dominated by two f–f transitions: $^4G_{5/2} \rightarrow {}^6H_{7/2}$ and $^4G_{5/2} \rightarrow {}^6H_{9/2}$, whereas the luminescence of **Eu$_2$Ti$_7$** is predominantly driven by the $^5D_0 \rightarrow {}^7F_2$ transition. The emission peak widths of **Sm$_2$Ti$_7$** are broader compared to **Eu$_2$Ti$_7$**, indicating higher color purity for **Eu$_2$Ti$_7$**.

Under daylight, the crystal samples of **Sm$_2$Ti$_7$** and **Eu$_2$Ti$_7$** appear colorless, but exhibit red luminescence when exposed

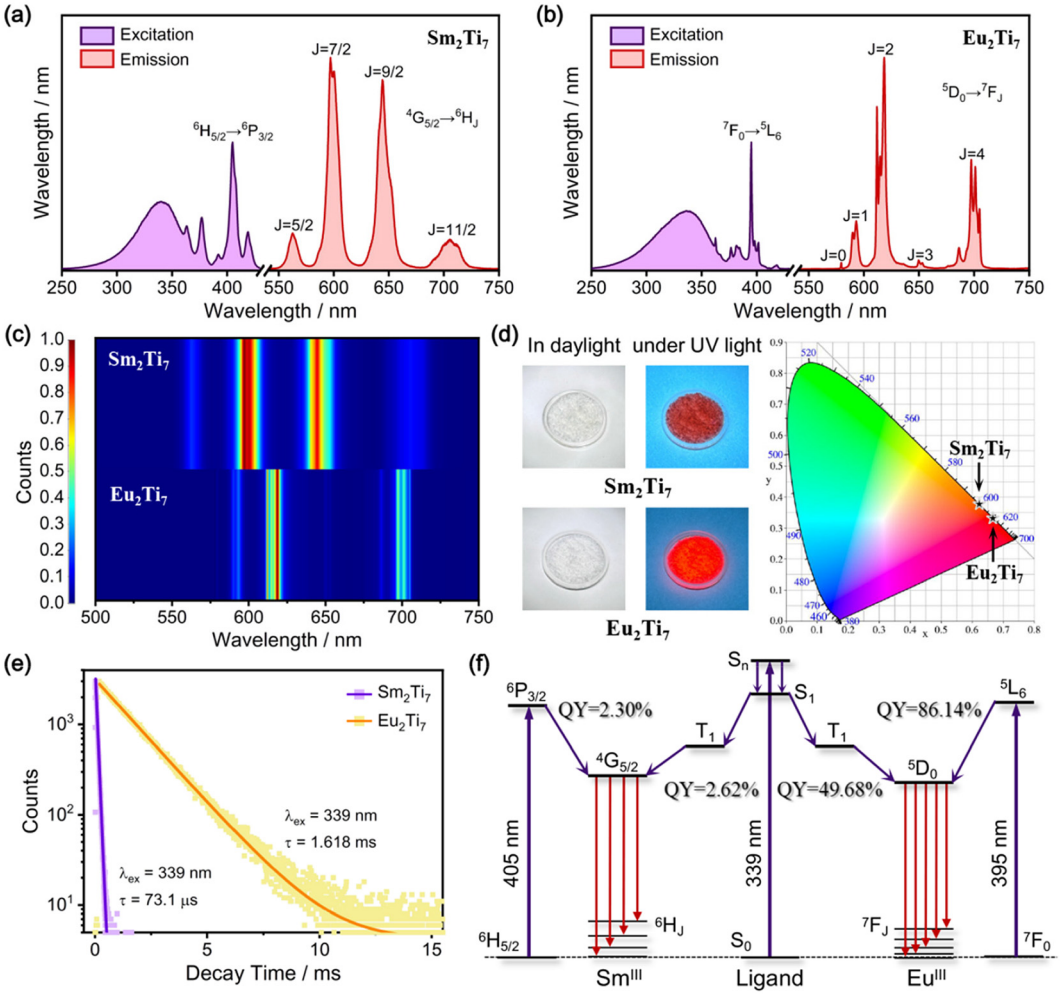

Fig. 2 (a) Excitation and emission spectra of **Sm$_2$Ti$_7$**. (b) Excitation and emission spectra of **Eu$_2$Ti$_7$**. (c) Relative emission intensities of **Sm$_2$Ti$_7$** and **Eu$_2$Ti$_7$**. (d) Physical photographs and CIE color coordinates of **Sm$_2$Ti$_7$** and **Eu$_2$Ti$_7$**. (e) Excited-state decay curves of **Sm$_2$Ti$_7$** and **Eu$_2$Ti$_7$**. (f) Quantum yield results of **Sm$_2$Ti$_7$** and **Eu$_2$Ti$_7$**.

Published on 21 November 2024. Downloaded on 5/17/2026 11:32:44 AM.

to ultraviolet light. The CIE color coordinates for **Sm_2Ti_7** are (x = 0.6179, y = 0.3815), and for **Eu_2Ti_7** are (x = 0.6632, y = 0.3365). Both coordinates fall within the orange-red region of the CIE chromaticity diagram, consistent with the observed luminescence. Notably, there is a visible difference in luminous intensity between the two samples, with **Eu_2Ti_7** exhibiting significantly stronger emission than **Sm_2Ti_7** (Fig. 2d). The excited-state decay curves, presented in Fig. 2e, indicate lifetimes of 72.6 μs (χ^2 = 1.1564) for **Sm_2Ti_7** and 1.618 ms (χ^2 = 1.0182) for **Eu_2Ti_7**.

The photo-luminescence process in lanthanide coordination system generally involves three stages: energy absorption, energy transfer to the Ln(III) emission level, and the subsequent f–f transitions that produce luminescence. Energy absorption occurs primarily through photosensitive ligands or intrinsic f–f transitions of Ln(III). Different absorption modes correspond to distinct energy transfer pathways.[17] In the first case, upon the ligand's absorption of energy, the energy populates the excited singlet energy level (S_n) of the ligand. Subsequently, it relaxes to the lowest singlet energy level (S_1) of the ligand. Then, intersystem crossing (ISC) takes place, leading to the energy populating the lowest triplet energy level (T_1) of the ligand. Afterwards, energy is transferred from the T_1 level to the excited state energy level of Ln(III). Once the energy reaches the emission energy level of Ln(III), radiative emission occurs. In the second case, Ln(III) absorbs energy *via* its intrinsic f–f transition, attaining a high excited state energy level of Ln(III). Subsequently, the energy relaxes to the emission level of Ln(III) through a non-radiative decay process and then radiative emission takes place. In the excitation spectra of **Sm_2Ti_7** and **Eu_2Ti_7**, strong and broad excitation peaks are attributed to ligand-based energy absorption, while strong but narrow excitation peaks arise from direct f–f transitions. Quantum yields (QYs) for **Sm_2Ti_7** and **Eu_2Ti_7** were measured for the two excitation modes at their strongest excitation wavelengths (Fig. 2f). Under ligand-sensitized excitation (339 nm), the QYs of **Sm_2Ti_7** and **Eu_2Ti_7** are 2.62% and 49.68%, respectively. For **Sm_2Ti_7**, when excited by the strongest f–f transition $^6H_{5/2} \rightarrow {}^6P_{3/2}$ (excitation wavelength at 405 nm), the QY is 2.30%. For **Eu_2Ti_7**, when excited by the strongest f–f transition $^7F_0 \rightarrow {}^5L_6$ (excitation wavelength at 395 nm), the QY is 86.14%.

Luminescence studies reveal that **Eu_2Ti_7** exhibits stronger emission intensity, higher color purity red light, longer luminescence lifetime and higher luminescence efficiency, compared to **Sm_2Ti_7** (Table 1). The difference in luminescence performance between **Eu_2Ti_7** and **Sm_2Ti_7** can be understood by analyzing their energy levels. When considering the ligand sensitization pathway, the emission levels of Sm(III) and Eu(III) are quite close ($^4G_{5/2}$: 17 924 cm^{-1}; $^5D_0$: 17 286 cm^{-1}). This suggests that the ligand absorption and energy transfer processes leading to the emission levels should be similar in both **Sm_2Ti_7** and **Eu_2Ti_7**. However, the lower QY of **Sm_2Ti_7** points to significant energy loss during the transition from the emission level ($^4G_{5/2}$) to the lower levels (^6H_J). A comparison of energy level diagrams reveals that Eu(III) transitions directly from the $^5D_0$ level to the ^7F_J levels without intermediate excited states. In contrast, Sm(III) has additional intermediate states (^6F_J) between the $^4G_{5/2}$ and ^6H_J levels. These intermediate states allow for non-radiative decay, contributing to energy loss and negatively impacting the luminescence of Sm(III). Interestingly, f–f transitions from the ground state ($^6H_{5/2}$) to these intermediate excited state levels were observed in the diffuse reflection spectrum of **Sm_2Ti_7**, showing strong absorption in the near-infrared region (Fig. S9c†).

Stability in solution

Eu_2Ti_7 was chosen as a representative to validate the stability of **Ln_2Ti_7** in dichloromethane (CH_2Cl_2). Dynamic light scattering (DLS) analysis revealed an average particle size of **Eu_2Ti_7** at 2.1 ± 0.5 nm (Fig. 3a), consistent with the theoretical particle size determined by single crystal structure analysis. To further assess the stability of **Eu_2Ti_7**, emission spectra were characterized at various concentrations, ranging from 10^{-2} to 10^{-5} M. The large solubility range benefits from the modification of the *tert*-butyl groups on the ligands. The results showed that the **Eu_2Ti_7** solution emits red light under ultraviolet irradiation, with emission peaks consistent with the characteristic Eu(III) transitions observed in the solid state (Fig. 3b). As the concentration decreased, the emission intensity weakened, but the spectral shape and peak positions remained unchanged. This consistency suggests that **Eu_2Ti_7** retains its structural integrity in CH_2Cl_2. Interestingly, after allowing the CH_2Cl_2 solution of **Eu_2Ti_7** to evaporate, colorless block crystals formed. SCXRD analysis confirmed that these crystals were **Eu_2Ti_7**, but with a change in space group from $C2/c$ to $P\bar{1}$ (Fig. 3c), likely due to the incorporation of CH_2Cl_2 molecules into the crystal lattice (Fig. S1c†). The recrystallized of **Eu_2Ti_7** also highlights the solubility and stability in CH_2Cl_2.

Magneto-optical response

Given the remarkable luminescence properties and high stability of **Eu_2Ti_7**, the magnetic circularly polarized luminescence

Table 1 Results of the luminescence properties of **Ln_2Ti_7**

Ln_2Ti_7	f–f transitions & emission peaks	CIE	Lifetime	QY (Ex)
Sm_2Ti_7	$^4G_{5/2} \rightarrow {}^6H_J$ 562 nm (J = 5/2), 597 nm (J = 7/2), 644 nm (J = 9/2), 706 nm (J = 11/2)	(x = 0.6179, y = 0.3815)	72.6 μs	2.3% (405 nm), 2.6% (339 nm)
Eu_2Ti_7	$^5D_0 \rightarrow {}^7F_J$ 580 nm (J = 0), 593 nm (J = 1), 618 nm (J = 2), 650 nm (J = 3), 701 nm (J = 4)	(x = 0.6632, y = 0.3365)	1.618 ms	86.1% (395 nm), 49.7% (339 nm)

This journal is © the Partner Organisations 2025

Published on 21 November 2024. Downloaded on 5/17/2026 11:32:44 AM.

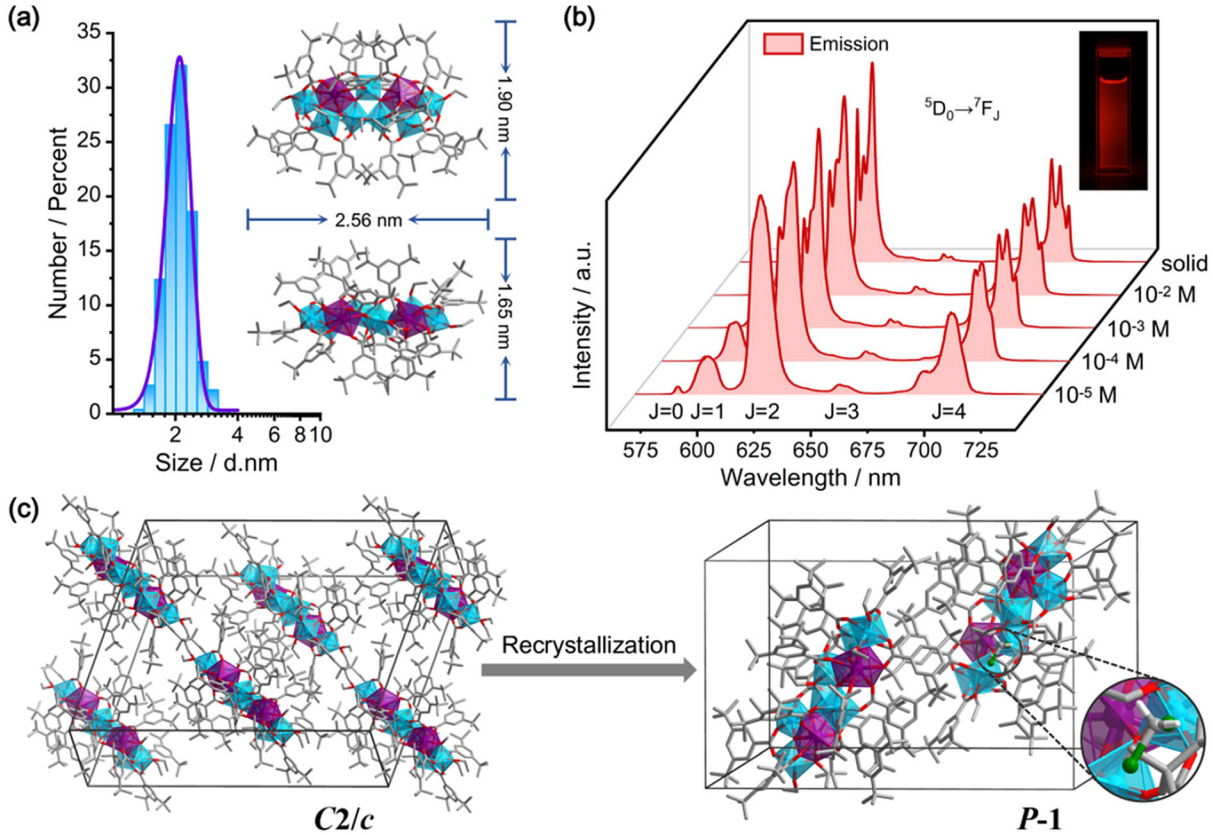

Fig. 3 (a) Dynamic light scattering analysis of Eu_2Ti_7. (b) Emission spectra of Eu_2Ti_7 solutions at various concentrations. (c) The space group transitioned from *C*2/*c* to *P*$\bar{1}$ after recrystallization of Eu_2Ti_7.

(MCPL) properties were studied in CH_2Cl_2 solution under an external magnetic field of 1.6 T. A CH_2Cl_2 solution of Eu_2Ti_7 with a concentration of 1×10^{-3} M was prepared. As illustrated in Fig. 4a, Eu_2Ti_7 displays distinct MCPL spectra ($^5D_0 \rightarrow {}^7F_J$) upon excitation at 328 nm (Fig. S7†), with significant CPL signals (ΔI) observed in the wavelength ranges of 585–605 nm (J = 1), 605–630 nm (J = 2) and 675–715 nm (J = 4), corresponding to the overall emission (I). The signals are primarily dominated by Faraday *A*-term.[18] In contrast, the Eu_2Ti_7 in solution did not show the CPL signal in the absence of an external magnetic field, confirming that the external magnetic field induces the CPL signal of achiral Eu_2Ti_7. The MCPL spectra under the N-up and S-up magnetic fields are nearly mirror images of each other.

To quantitatively analyze the MCPL results for different f–f transitions of Eu_2Ti_7, the luminescence asymmetry factor g_{lum} ($g_{lum} = \Delta I/I$) is used.[19] In MCPL, the g_{lum} value should be normalized by the magnetic flux density (B) of the external magnetic field, giving $g_{MCPL} = g_{lum}/B$ (T^{-1}). The g_{lum} values for Eu_2Ti_7 are presented in Fig. 4b, with the peak values summarized in Table S3.† For chiral Eu(III)-contained systems without an external magnetic field, the largest g_{lum} value typically occurs during the magnetic dipole transition $^5D_0 \rightarrow {}^7F_1$. However, in Eu_2Ti_7, the magnetic field has the greatest influence on the electric dipole transition $^5D_0 \rightarrow {}^7F_4$, followed by the magnetic dipole transition $^5D_0 \rightarrow {}^7F_1$, and then the electric dipole transition $^5D_0 \rightarrow {}^7F_2$. The maximum $|g_{MCPL}|$ for the $^5D_0 \rightarrow {}^7F_4$ transition is observed at 709 nm with a value of 4.0×10^{-2} T^{-1}. For the $^5D_0 \rightarrow {}^7F_1$ transition, the maximum $|g_{MCPL}|$ is 1.5×10^{-2} T^{-1} at 586 nm. Lastly, for the $^5D_0 \rightarrow {}^7F_2$ transition, the maximum $|g_{MCPL}|$ is 0.8×10^{-4} T^{-1} at 625 nm. In contrast, accurate MCPL analysis for Sm_2Ti_7 was not feasible due to its weak emission intensity and the interference of background noise. This highlights the necessity of strong luminescence intensity as a prerequisite for effective MCPL measurement.

Although the suboptimal luminescence of Sm_2Ti_7 hinders obtaining a clear MCPL signal, its strong absorption (arising from $^6H_{5/2} \rightarrow {}^6F_{1/2-11/2}$ transitions) in the near-infrared region is of highly significant for magnetic circular dichroism (MCD) studies. As shown in Fig. 4d, the CD signals (ΔA) for Sm_2Ti_7 were recorded at the external magnetic field strength of 1.6 T, corresponding to the overall absorption (A). When the magnetic field direction was reversed, the CD signals maintain the magnitude but exhibit a mirrored distribution. The MCD results were further analyzed by calculating the g_{MCD} factor, defined as $g_{MCD} = g_{abs}/B$ (where $g_{abs} = \Delta A/A$ is the absorption asymmetry factor[20]). For Sm_2Ti_7, the maximum $|g_{MCD}|$ value is 2.1×10^{-2} T^{-1} at 1102 nm, corresponding to the electric dipole transition $^6H_{5/2} \rightarrow {}^6F_{9/2}$. Additionally, for the electric dipole transition $^6H_{5/2} \rightarrow {}^6F_{11/2}$, the magnetic dipole transition $^6H_{5/2}$

Published on 21 November 2024. Downloaded on 5/17/2026 11:32:44 AM.

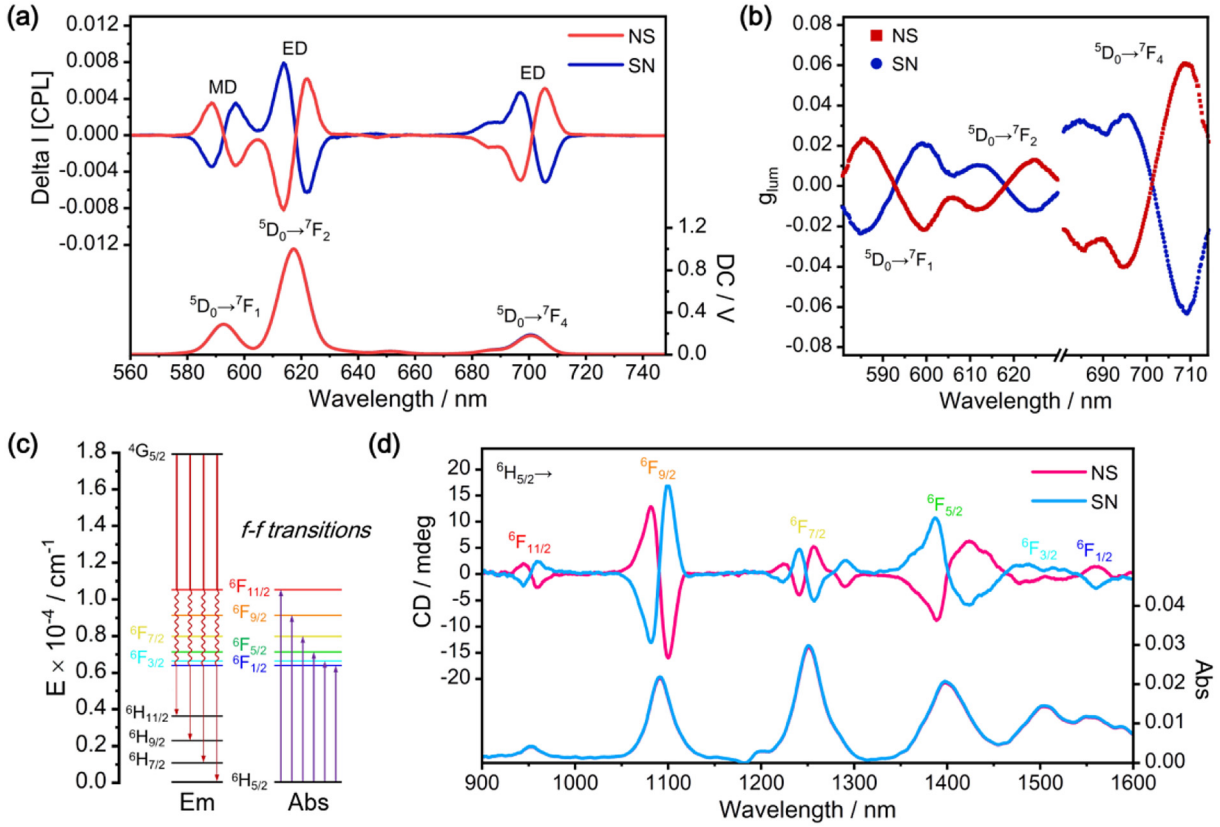

Fig. 4 (a) The MCPL (upper) and PL (lower) spectra of $\mathbf{Eu_2Ti_7}$ in solution state under the 1.6 T external magnetic field. (b) Correspondence between g_{lum} value and wavelength in MCPL of $\mathbf{Eu_2Ti_7}$. (c) Energy level diagram of emission and absorption f–f transitions for Sm(III). (d) The near-infrared MCD (upper) and absorption (lower) spectra of $\mathbf{Sm_2Ti_7}$ in solution state under the 1.6 T external magnetic field.

$\rightarrow {}^6F_{5/2}$ and the magnetic dipole transition $^6H_{5/2} \rightarrow {}^6F_{3/2}$, the maximum $|g_{MCD}|$ values of these transitions are on the order of 10^{-2} T^{-1}.

Conclusion

In conclusion, we report a series of isostructural LTOCs $\mathbf{Ln_2Ti_7}$ (Ln = La, Sm, Eu), using 3,5-di-*tert*-butylbenzoic acid serving as the ligand. A detailed comparative analysis of the luminescence properties revealed that $\mathbf{Eu_2Ti_7}$ exhibits significantly superior luminescence characteristics compared to $\mathbf{Sm_2Ti_7}$, including stronger emission intensity, higher quantum yield, and longer lifetime. We also conducted a study of the magnetic circularly polarized luminescence (MCPL) of $\mathbf{Eu_2Ti_7}$, demonstrating its responsiveness to external magnetic fields and showcasing its potential for magneto-optical applications. The energy-level analysis explaining the luminescence differences between $\mathbf{Eu_2Ti_7}$ and $\mathbf{Sm_2Ti_7}$ further motivated our research into the magnetic circular dichroism (MCD) properties of $\mathbf{Sm_2Ti_7}$, particularly in the near-infrared region. This study not only contributes to the understanding of magneto-optical effects in lanthanide-based clusters but also emphasizes the importance of analyzing the energy levels of Ln(III) ions for advancing magneto-optical research.

Data availability

All relevant data are within the manuscript and ESI.† The data are available from the corresponding author on reasonable request.

Conflicts of interest

There are no conflicts to declare.

Acknowledgements

We are grateful for the financial support from the National Natural Science Foundation of China (Grant No. 92161104, 92161203, and 92361301).

References

1 P. S. Peijzel, A. Meijerink, R. T. Wegh, M. F. Reid and G. W. Burdick, A complete $4f^n$ energy level diagram for all trivalent lanthanide ions, *J. Solid State Chem.*, 2005, **178**, 448–453.

 This journal is © the Partner Organisations 2025

Published on 21 November 2024. Downloaded on 5/17/2026 11:32:44 AM.

2 (*a*) P. Chen, B. Peng, Z. Liu, J. Liu, D. Li, Z. Li, X. Xu, H. Wang, X. Zhou and T. Zhai, Room-Temperature Magnetic-Induced Circularly Polarized Photoluminescence in Two-Dimensional Er_2O_2S, *J. Am. Chem. Soc.*, 2024, **146**, 6053–6060; (*b*) C. Li, L. C. Adi, K. Paillot, I. Breslavetz, L. Long, L. Zheng, G. L. J. A. Rikken, C. Train, X. Kong and M. Atzori, Enhancement of Magneto-Chiral Dichroism Intensity by Chemical Design: The Key Role of Magnetic-Dipole Allowed Transitions, *J. Am. Chem. Soc.*, 2024, **146**, 16389–16393; (*c*) H. Wang, B. Yin, J. Bai, X. Wei, W. Huang, Q. Chang, H. Jia, R. Chen, Y. Zhai, Y. Wu and C. Zhang, Giant magneto-photoluminescence at ultralow field in organic microcrystal arrays for on-chip optical magnetometer, *Nat. Commun.*, 2024, **15**, 3995; (*d*) Y. Li, H. Wang, Z. Zhu, Y. Wang, F. Liang and H. Zou, Aggregation induced emission dynamic chiral europium(III) complexes with excellent circularly polarized luminescence and smart sensors, *Nat. Commun.*, 2024, **15**, 2896.

3 H. Yoshikawa, G. Nakajima, Y. Mimura, T. Kimoto, Y. Kondo, S. Suzuki, M. Fujiki and Y. Imai, Mirror-image magnetic circularly polarized luminescence (MCPL) from optically inactive EuIII and TbIIItris(β-diketonate), *Dalton Trans.*, 2020, **49**, 9588–9594.

4 (*a*) B. Han, X. Gao, J. Lv and Z. Tang, Magnetic Circular Dichroism in Nanomaterials: New Opportunity in Understanding and Modulation of Excitonic and Plasmonic Resonances, *Adv. Mater.*, 2018, **32**, 1801491; (*b*) B. Han, X. Gao, J. Lv and Z. Tang, Magnetic Circular Dichroism in Nanomaterials: New Opportunity in Understanding and Modulation of Excitonic and Plasmonic Resonances, *Adv. Mater.*, 2018, **32**, 1801491.

5 (*a*) D. A. Gálico, C. M. S. Calado and M. Murugesu, Lanthanide molecular cluster-aggregates as the next generation of optical materials, *Chem. Sci.*, 2023, **14**, 5827–5841; (*b*) Y. Li, H. Wang, Z. Zhu, F. Liang and H. Zou, Recent advances in the structural design and regulation of lanthanide clusters: Formation and self-assembly mechanisms, *Coord. Chem. Rev.*, 2023, **493**, 215322; (*c*) X. Zheng, J. Xie, X. Kong, L. Long and L. Zheng, Recent advances in the assembly of high-nuclearity lanthanide clusters, *Coord. Chem. Rev.*, 2019, **378**, 222–236.

6 (*a*) L. Armelao, S. Quici, F. Barigelletti, G. Accorsi, G. Bottaro, M. Cavazzini and E. Tondello, Design of luminescent lanthanide complexes: From molecules to highly efficient photo-emitting materials., *Coord. Chem. Rev.*, 2010, **254**, 487–505; (*b*) A. de Bettencourt-Dias and J. S. K. Rossini, Ligand Design for Luminescent Lanthanide-Containing Metallopolymers, *Inorg. Chem.*, 2016, **55**, 9954–9963; (*c*) J.-C. G. Bünzli and C. Piguet, Taking advantage of luminescent lanthanide ions, *Chem. Soc. Rev.*, 2005, **34**, 1048–1077; (*d*) Y. Hasegawa, Y. Kitagawa and T. Nakanishi, Effective photosensitized, electrosensitized, and mechanosensitized luminescence of lanthanide complexes, *NPG Asia Mater.*, 2018, **10**, 52–70.

7 (*a*) C. Huang, R. Sun, L. Bao, X. Tian, C. Pan, M. Li, W. Shen, K. Guo, B. Wang, X. Lu and S. Gao, A hard molecular nanomagnet from confined paramagnetic 3d-4f spins inside a fullerene cage, *Nat. Commun.*, 2023, **14**, 8443; (*b*) Z. Lu, Z. Zhuo, W. Wang, Y. Huang and M. Hong, $\{Gd_{44}Ni_{22}\}$: a gigantic 3d–4f wheel-like nanoscale cluster with a large magnetocaloric effect, *Inorg. Chem. Front.*, 2023, **10**, 979–983; (*c*) X. Wang, S. Wang, J. Chen, J. Jia, C. Wang, K. Paillot, I. Breslavetz, L. Long, L. Zheng, G. L. J. A. Rikken, C. Train, X. Kong and M. Atzori, Magnetic 3d–4f Chiral Clusters Showing Multimetal Site Magneto-Chiral Dichroism, *J. Am. Chem. Soc.*, 2022, **144**, 8837–8847.

8 (*a*) K. Mishima, D. Kaji, M. Fujiki and Y. Imai, Remarkable Effects of External Magnetic Field on Circularly Polarized Luminescence of EuIII$(hfa)_3$ with Phosphine Chirality, *ChemPhysChem*, 2021, **22**, 1728–1737; (*b*) F. S. Richardson and H. G. Brittain, A structural study of tris(.beta.-diketonate)europium(III) complexes in solution using magnetic circularly polarized luminescence spectroscopy, *J. Am. Chem. Soc.*, 1981, **103**, 18–24.

9 D. A. Gálico and M. Murugesu, Magnetic Circularly Polarized Luminescence with Heterometallic Molecular Cluster–Aggregates, *Adv. Opt. Mater.*, 2024, **12**, 2401064.

10 (*a*) J. Chen, K. Huang, P. Cheng, M. Qi, H. Xu, J. Chen, Y. Duan, X. Kong, L. Zheng and L. Long, Strong NIR-II Magneto-Optical Activity of a Chiral $Sm_{15}Cu_{54}$ Cage, *J. Am. Chem. Soc.*, 2024, **146**, 22913–22917; (*b*) Y. Kitagawa, S. Wada, K. Yanagisawa, T. Nakanishi, K. Fushimi and Y. Hasegawa, Molecular Design Guidelines for Large Magnetic Circular Dichroism Intensities in Lanthanide Complexes, *ChemPhysChem*, 2016, **17**, 845–849.

11 (*a*) C. Artner, S. Kronister, M. Czakler and U. Schubert, Ion-Size-Dependent Formation of Mixed Titanium/Lanthanide Oxo Clusters, *Eur. J. Inorg. Chem.*, 2014, **2014**, 5596–5602; (*b*) W. Fang, L. Zhang and J. Zhang, Synthetic strategies, diverse structures and tuneable properties of polyoxo-titanium clusters, *Chem. Soc. Rev.*, 2018, **47**, 404–421; (*c*) Y. Liu, W. Fang, L. Zhang and J. Zhang, Recent advances in heterometallic polyoxotitanium clusters, *Coord. Chem. Rev.*, 2020, **404**, 213099; (*d*) S. Wang, H. Su, L. Yu, X. Zhao, L. Qian, Q. Zhu and J. Dai, Fluorescence and energy transfer properties of heterometallic lanthanide-titanium oxo clusters coordinated with anthracenecarboxylate ligands, *Dalton Trans.*, 2015, **44**, 1882–1888; (*e*) G. Zhang, S. Wang, J. Hou, C. Mo, C. Que, Q. Zhu and J. Dai, A lanthanide-titanium ($LnTi_{11}$) oxo-cluster, a potential molecule based fluorescent labelling agent and photocatalyst, *Dalton Trans.*, 2016, **45**, 17681–17686.

12 (*a*) R. Chen, Z. Hong, Y. Zhao, H. Zheng, G. Li, Q. Zhang, X. Kong, L. Long and L. Zheng, Ligand-Dependent Luminescence Properties of Lanthanide-Titanium Oxo Clusters, *Inorg. Chem.*, 2019, **58**, 15008–15012; (*b*) G. Li, L. Long, X. Kong and L. Zheng, Recent Advances in Lanthanide-titanium-oxo Clusters, *Chem. J. Chin. Univ.*, 2020, **40**, 2577–2586; (*c*) W. Liu, G. Li, H. Xu, Y. Deng, M. Du, L. Long, L. Zheng and X. Kong, Circularly polarized luminescence and performance modulation of chiral euro-

Published on 21 November 2024. Downloaded on 5/17/2026 11:32:44 AM.

pium-titanium (Eu_2Ti_4)-oxo clusters, *Chem. Commun.*, 2023, **59**, 346–349; (*d*) D. Lu, Z. Hong, J. Xie, X. Kong, L. Long and L. Zheng, High-Nuclearity Lanthanide-Titanium Oxo Clusters as Luminescent Molecular Thermometers with High Quantum Yields, *Inorg. Chem.*, 2017, **56**, 12186–12192; (*e*) X. Shu, W. Luo, H. Wang, M. Fu, Q. Zhu and J. Dai, Eu-phen Bonded Titanium Oxo-Clusters, Precursors for a Facile Preparation of High Luminescent Materials and Films, *Inorg. Chem.*, 2020, **59**, 10422–10429; (*f*) Y. Zhao, H. Zheng, L. Chen, H. Chen, X. Kong, L. Long and L. Zheng, The Effect on the Luminescent Properties in Lanthanide-Titanium OXO Clusters, *Inorg. Chem.*, 2019, **58**, 10078–10083.

13 (*a*) C. Liu and Y. Wang, Supramolecular Chemistry of Titanium Oxide Clusters, *Chem. – Eur. J.*, 2021, **27**, 4270–4282; (*b*) L. Zhang, X. Fan, X. Yi, X. Lin and J. Zhang, Coordination-Delayed-Hydrolysis Method for the Synthesis and Structural Modulation of Titanium-Oxo Clusters, *Acc. Chem. Res.*, 2022, **55**, 3150–3161.

14 C. Wang, J. Zhang and X. Zhu, Synthesis of lanthanide-doped titanium-oxo clusters for efficient photocurrent responses, *J. Solid State Chem.*, 2021, **304**, 122586.

15 (*a*) S. S. Mortensen, M. A. M. Nielsen, P. Nawrocki and T. J. Sørensen, Electronic Energy Levels and Optical Transitions in Samarium(III) Solvates, *J. Phys. Chem. A*, 2022, **126**, 8596–8605; (*b*) M. Tang, Z. Zhu, Y. Li, W. Qin, F. Liang, H. Wang and H. Zou, Specific smart sensing of electron-rich antibiotics or histidine improves the antenna effect, luminescence, and photodynamic sterilization capabilities of lanthanide polyoxometalates, *J. Colloid Interface Sci.*, 2025, **680**, 235–246.

16 K. Binnemans, Interpretation of europium(III) spectra, *Coord. Chem. Rev.*, 2015, **295**, 1–45.

17 (*a*) E. G. Moore, A. P. S. Samuel and K. N. Raymond, From Antenna to Assay: Lessons Learned in Lanthanide Luminescence, *Acc. Chem. Res.*, 2009, **42**, 542–552; (*b*) J. Xu and S. Tanabe, Persistent luminescence instead of phosphorescence: History, mechanism, and perspective, *J. Lumin.*, 2019, **205**, 581–620; (*c*) A. d. Bettencourt-Dias, *Luminescence of Lanthanide Ions in Coordination Compounds and Nanomaterials*, WILEY, 2014, ISBN 978-1119950837; (*d*) B. Yu, Z. Zhu, W. Qin, H. Wang, Y. Li, F. Liang and H. Zou, Enhancement of Luminescence, Multiple-Sensing, and Differentiated Live-Cell-Imaging Properties of High-Nuclear Lanthanide Nanoclusters via the Zn(II)-Chelate-Controlled Dual Antenna Effect, *ACS Mater. Lett.*, 2024, **6**, 3312–3326.

18 F. Zinna and G. Pescitelli, Magnetic Circularly Polarized Luminescence of Organic Compounds, *Eur. J. Org. Chem.*, 2023, e202300509.

19 Z. Gong, Z. Li and Y. Zhong, Circularly polarized luminescence of coordination aggregates, *Aggregate*, 2022, **3**, e177.

20 C. Zhang, S. Li, X. Dong and S. Zang, Circularly polarized luminescence of agglomerate emitters, *Aggregate*, 2021, **2**, e48.

 This journal is © the Partner Organisations 2025